ChemComm
Chemical Communications

Accepted Manuscript

This article can be cited before page numbers have been issued, to do this please use: H. Pan, B. Zheng, H. Shen, M. Qi, Y. Shang, C. Wu, R. Zhu, L. Cheng and Q. Wang, *Chem. Commun.*, 2020, DOI: 10.1039/D0CC00326C.

ROYAL SOCIETY OF CHEMISTRY

rsc.li/chemcomm

View Article Online
DOI: 10.1039/D0CC00326C

COMMUNICATION

Strength-tunable Printing of Xanthan gum Hydrogel via Enzymatic Polymerization and Amide Bioconjugation†

Received 00th January 20xx,
Accepted 00th January 20xx

DOI: 10.1039/x0xx00000x

Hui Pan[#a], Bolin Zheng[#b], Hongdou Shen[a], Meiyuan Qi[a], Yinghui Shang[a], Chu Wu[a], Rongrong Zhu[b], Liming Cheng[b] and Qigang Wang [*a b]

Amide bioconjugation and interfacial enzyme polymerization are designed to provide a general strategy for regulating the mechanical strength (storage modulus from 3kPa to 100kPa) of printable hydrogel inks.

Hydrogels are soft-wet materials made up of three-dimensional hydrophilic macromolecular networks. Due to their water-rich microenvironment and tuneable strength, polymer hydrogels with hydrophilic network have attracted emerging attention as scaffolds in biocatalysis[1-5], biomedicine[6-7] and tissue engineering fields [8-12]. Materials used for the preparation of polymer hydrogel can be either from natural or synthetic sources[13-17]. Natural protein/polysaccharide hydrogels with reversible physical interactions are shear-thinning and thus printable[18-19], but lack of mechanical strength[20-21]. The typical polymer hydrogels formed by the copolymerization of monomers and multivinyl crosslinker are tough, but non-processable due to their significantly viscosity increasement around gel point[22-26]. Therefore, the combination of the strength performance of synthetic polymer and the printable ability of non-covalent system is a reasonable approach for fabricating tough and printable polymer-composite hydrogels[27-28]. Liu and co-workers have demonstrated that poly (*N*-acryloyl glycinamide) hydrogels with remarkable supramolecular hydrogen bonds can be printed via the reversible sol-gel transition at high temperature[29]. Zhao and co-workers have utilized the viscous clay as printable matrix to execute photo-polymerization for strength regulation[30]. As deduced from these pioneered literatures, we know that the contradiction of in-situ polymerization and stable extrusion is the constraining factor for ensuring the stable viscosity and successful printing.

Herein, a dual-nozzle extrusive printing model was employed to avoid the mutual effect between polymerization and extrusion. The natural polysaccharide xanthan gum is utilized as the stable 3D printing framework in both nozzles. The interfacial enzyme polymerization is triggered by the separated loading of enzymes and substrates within different nozzle. In general, enzymatic polymerization is usually nontoxic[31-33]. The selected Glucose oxidase (GOx)/glucose/N-Hydroxy sulfosuccinimide (Sulfo-NHS) system can quickly produce nitrogen radical and trigger polymerization in the absence of oxygen. Enzymatic polymerization can be regulated by the interface diffusion of enzymes and substrates. In our dual-nozzle extrusive mode, the interfacial polymerization can be achieved through mutual penetration after printing. Amide-bond bioconjugation by Sulfo-NHS and EDC·HCl is another widely used biological modification technique[34], which can interact slowly and regulatably between the amino and carboxyl group. At the same time, due to the presence of carboxyl or amino groups, natural polymers, like xanthan gum, biologically active guest bodies, and even cells are readily coupled to poly (*N*-acryloyl-L-lysine) without additional modification. As a result, our printable polymer hydrogel platforms offer advantages such as adjustable strength, no modification was required for most bio-inks and a comprehensive biological approach that can be potentially

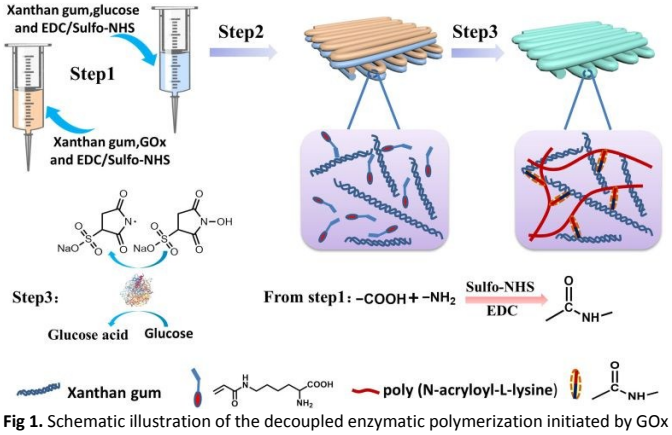

Fig 1. Schematic illustration of the decoupled enzymatic polymerization initiated by GOx

[a.] *School of Chemical Science and Engineering, Tongji University, Shanghai 200092, China. E-mail: wanggq66@tongji.edu.cn.*
[b.] *Key Laboratory of Spine and Spinal Cord Injury Repair and Regeneration of Ministry of Education, Orthopaedic Department of Tongji Hospital, School of Medicine, Tongji University, 389 Xincun Road, 200065 Shanghai, P. R. China*
 # These authors contributed equally to this work and should be considered co-first authors.
Electronic Supplementary Information (ESI) available: See DOI: 10.1039/x0xx00000x

View Article Online DOI: 10.1039/D0CC00326G

/ glucose / Sulfo-NHS, the gelation by cross-linking of EDC·HCl and Sulfo-NHS and dual-nozzle extrusion printing.

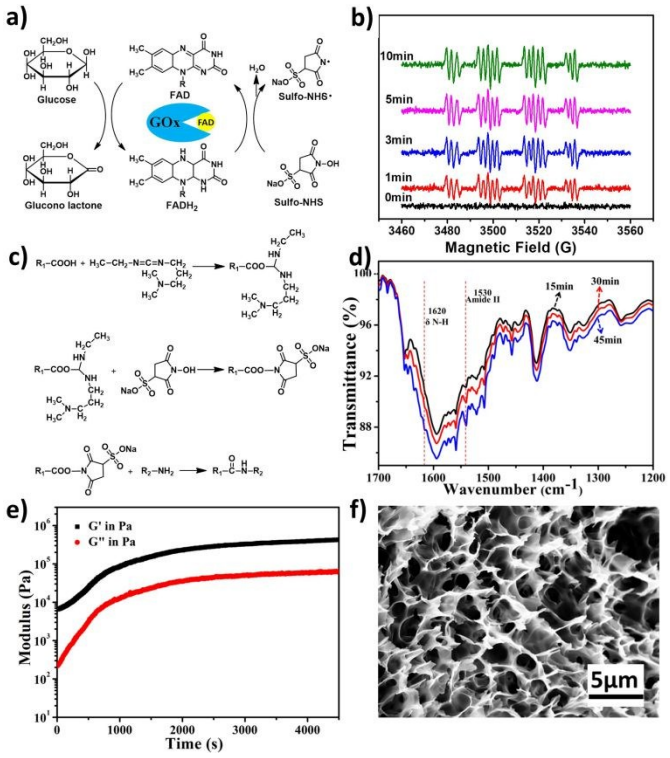

Fig. 2 (a) Schematic diagram of the anaerobic catalysis mechanism of GOx in our gelation system. (b) EPR spectrums of radical catalyzed by GOx/glucose with DMPO as the spin trap. (c) Schematic diagram of EDC·HCl /sulfo-NHS crosslink mechanism amino and carboxyl groups (d) Infrared spectra of hydrogel at different times. (e) Dynamic time sweep tests of composite hydrogel. (f) SEM image of the hydrogel.

combined with biologically active guests.

All components were illustrated in Fig. 1, xanthan gum was used as the backbone and supporting material for 3D printing, the dual-nozzle extrusion process was used to regulate the gelation process of enzymatic polymerization. Our bio-printable hydrogel contains three functional components: gelling agent solution, enzyme initiation system, amide bioconjugate reagent. Xanthan gum with a mass concentration of 5% was selected as the printable skeleton, and 2-6wt% concentration of *N*-acryloyl-L-lysine solution was used as a polymerizable monomer, enzymatic polymerization was initiated by mutual penetration of GOx and glucose. In the bio-crosslinking system, the amount of EDC·HCl and *N*-acryloyl-L-lysine are varied to control the final degree of crosslinking, and the hydrogel was finally formed at room temperature.

To verify the mechanism of enzymatic polymerization, electron paramagnetic resonance (EPR) spectroscopy was performed to detect the existing radicals within the bio-initiated system of GOx (100U/ml)/glucose (50mg/ml)/Sulfo-NHS (10mg/ml). Similar to the reported GOx/glucose/NHS system[35], the anaerobic metabolism of glucose and Sulfo-NHS catalyzed by glucose oxidase can produce nitrogen radicals by hydroxyl reduction. Dimethyl pyridine N-oxide (DMPO) was employed to trap the unstable and short-life time free radicals to form a long-lived nitroxide for EPR characterization. As shown in Fig. 2b, the EPR spectrum of the initiated system without *N*-acryloyl-L-lysine demonstrated a sextet signal with *g* value of 2.0058, a^N = 1.95G, a^H =15.4G, which were coincident with the values of a DMPO trapped nitrogen centred radical. The signal of the propagating carbon radical (Fig. S2, ESI†) with *g* value of 2.0061 was also observed in the enzyme-initiated system containing with *N*-acryloyl-L-lysine. Therefore, our bio-initiated system could be used to mildly initate radical polymerization with high cytocompatibility compared to traditional heat or photo polymerization. In normal conditions, GOx catalyzes the production of glucono-lactone by glucose, the Sulfo-NHS was reduced as the hydrogen acceptor, which produces nitrogen free radicals under anaerobic conditions (Fig. 2a). Then these free radicals were transferred to form carbon radicals to initiate polymerization.

The carboxyl group in the polysaccharide could be biocoupled with the amino group on the *N*-acryloyl-L-lysine to crosslink. EDC·HCl can react with the carboxyl group on the polysaccharide to form an unstable urea derivative, and the stability of products crosslinked by EDC·HCl, was enhanced by Sulfo-NHS by the forming more stable ester (Fig. 2c). As shown in Fig. 2d, the conjugation process was observed by infrared spectroscopy, the vibration peak of amide- Ⅱ at 1530 cm^{-1} and N-H at 1620 cm^{-1} were increasing as the reaction progress. These indicate that the bioconjugation reaction of *N*-acryloyl-L-lysine with Xanthan gum continues to occur during gel formation. The polymerization process can also be monitored by nuclear magnetic resonance (NMR) characterization (Fig. S3, ESI†), the conversion test revealed that almost 90% of conversion of *N*-acryloyl-L-lysine was completed in one hour. The gelation process of composite hydrogels was monitored by dynamic time sweep test (Fig. 2e), the storage modulus G' and loss modulus G" increased rapidly within 900 seconds due to the quick enzymatic polymerization. The morphology of the hydrogel was investigated by scanning electron microscopy (SEM), as shown in Fig. 2f, the hydrogel had a uniform three-dimensional porous structure with pore sizes of 3-4 micron in the hydrogel matrix.

Since mechanical properties affect the formability of materials and the living environment of cells, proper mechanical strength is necessary for materials. Rheological studies of Xanthan gum, poly (*N*-acryloyl-L-lysine) hydrogel and composite hydrogel are shown in Fig. 3a, xanthan gum shows the lowest storage modulus G' and loss modulus G", which makes it easy to print, and the composite hydrogels exhibited the highest storage modulus G' and loss modulus G", this indicates that the composite hydrogels have gel-like rheological properties. Furthermore, the composite hydrogel with 0.5% EDC·HCl and 4% *N*-acryloyl-L-lysine showed good compression toughness. At 40% compression strain, the compression curve had almost no change after 10 times (Fig. 3b), and the compression modulus was about 23kPa. A series of composite hydrogels with various monomer content were prepared by the enzymatic polymerization (GOx (50U/ml)/glucose (10mg/ml)/Sulfo-NHS (5mg/ml).). As indicated in Fig. 3c, the compression modulus of composite hydrogels increased from 27.9 kPa to 52.1 kPa as the amount of monomer is increased from 2 wt% to 6 wt% with 0.5 wt% EDC·HCl. It can be

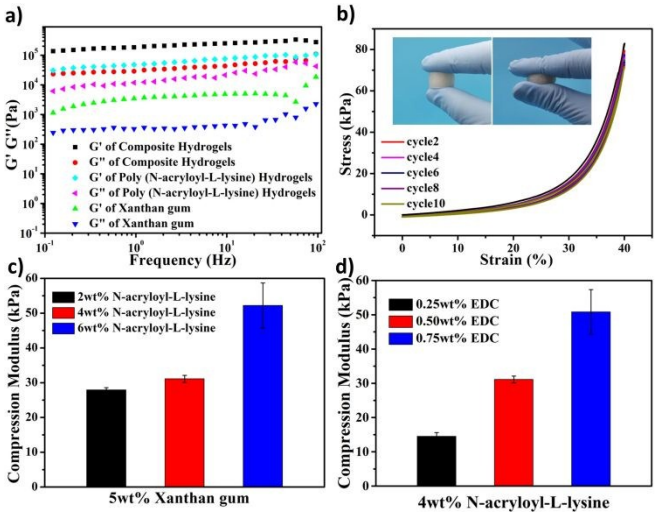

understood that the addition of the monomer increased the crosslinking density. The compression

Fig. 3 (a) Rheological assessment of xanthan gum, poly (*N*-acryloyl-L-lysine) hydrogel and composite hydrogel. (b) Cyclic compression test of Composite hydrogels (c) Compressive modulus of composite hydrogels with different *N*-acryloyl-L-lysine amounts. (d) Compressive modulus of hydrogels with different EDC·HCl amounts.

modulus of composite hydrogels increased from 14.5 kPa to 50.8 kPa as the amount of EDC·HCl increased from 0.25 wt% to 0.75 wt% with 4wt% *N*-acryloyl-L-lysine (Fig. 3d), and the tensile modulus of composite hydrogels increased from 8.03kPa to 35.4kPa (Fig. S4, ESI†). This can also be attributed to the increase in crosslinking density. Moreover, special cross-linking allows *N*-acryloyl-L-lysine to cross-link many other natural polymer containing amino or carboxyl groups. Various natural proteins or polysaccharides could be used to build hydrogel networks (Fig. S5, ESI†), and different natural polymer doping, which exhibits different mechanic strength. For example, the compression modulus increased from 1.0kPa to 4.4kPa as the amount of bovine serum albumin (BSA) increased from 4wt% to 10wt% with 4% *N*-acryloyl-L-lysine and 0.5% EDC·HCl (Fig. S6, ESI†). The same situation happens when carboxymethyl cellulose (CMC) is added (Fig. S7, ESI†). In summary , our hydrogels exhibited excellent mechanical properties and tunable strength after coupling with natural molecules.

Extrusion type 3D printing requires stable viscosity. However, enzyme-catalyzed free radical polymerization tends to cause a sharp rise in viscosity. In order to address these limitations, we have developed a new printing strategy. Our strategy incorporates two inks: Ink A prepared from glucose oxidase, *N*-acryloyl-L-lysine, EDC·HCl / Sulfo-NHS and xanthan gum, Ink B prepared from glucose, *N*-acryloyl-L-lysine, EDC·HCl / Sulfo-NHS and xanthan gum. As shown in Fig. 4a, when the one printhead prints a layer of ink A, the other printhead immediately prints the ink B on the pattern printed previously. Xanthan gum provides the suitable viscosity and printed skeleton for extrusion printing, subsequent infiltration of glucose and glucose oxidase initiates free radical polymerization to reinforce the printed skeleton. This printing method could accurately place interpenetrating hydrogel bundles and builds complex geometries. The dual-inks were compared with single ink by using two printing head, through the observation and comparison of SEM images, we could find

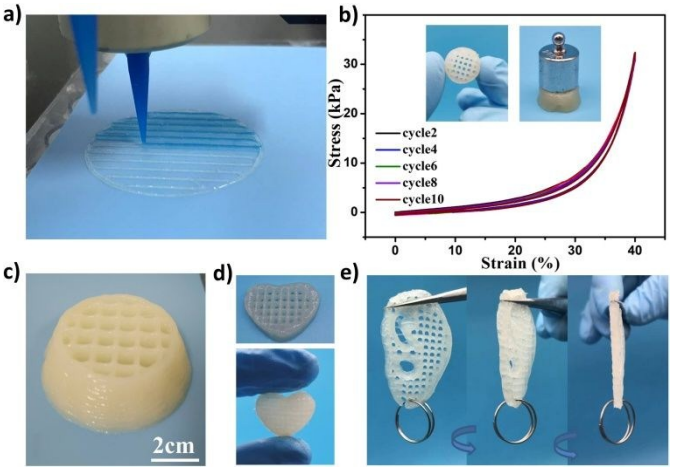

Fig. 4 (a) Printing method showing. (b) Cyclic compression experiment on the cylinder after printing. (c-e) 3D printing of composite hydrogels.

that the structure obtained by using ink A and ink B was slightly larger than that of a single ink, and the surface was smoother (Fig. S8, ESI†). The cylinder after printing underwent cyclic compression experiments showed good toughness (Fig 4b). At 40% compression strain, it cycles 10 times and the compression curve hardly changes. The printed round tables retained its structural integrity and the stacking of layers could be seen clearly (Fig. 4c). Furthermore, we also printed love model(25×20×5mm) and ears model (26×40×4 mm) (Fig. 4d,4e), the printed construct was stable and there has no deformation or collapse during the printing process. After we have finished printing for 60 minutes, the printed materials could be easily and completely removed. Through the Fig. 4e, the complete structure and obvious pores of the ear can be seen. These results show that the printing of double extrusion nozzle is very suitable for hydrogel formed by enzyme catalysis, xanthan gum provides appropriate viscosity for extrusion printing. The printed object shows a high precision, complete structure and obvious pores.

In vitro cytotoxicity assay and 3D cell culture were conducted to examine the biocompatibility of composite hydrogel. Composite hydrogels could load cells for bioprinting and is low-toxic to cells. Enzyme-catalyzed free radical polymerization is often mild and low-toxic. The hydrogels which were constructed with monomer obtained from natural lysine modified by acrylic acid, and crosslinked by amide bonds induced by low-toxic EDC·HCl and sulfo-NHS, exhibited high biocompatibility. NIH-3T3 cells from a mouse embryonic fibroblast cell line are chosen as the cell model. As shown in Fig. 5a, cell viability basically unchanged after co-incubation with gel powder, suggesting that this enzyme-initiated gelation system has relatively low cytotoxicity. Cell viability was assessed by fluorescent staining. After co-culture with different concentrations of gel powders (0, 1, 10 and 100 μg/mL) for 24h and 48h, living cells were bright green fluorescence while dead cells were stained with red fluorescence on fluorescent inverted microscope views. To our delight, few dead cells are observed. Our results indicate that

NIH-3T3 cells maintained high survival rates after co-culturing

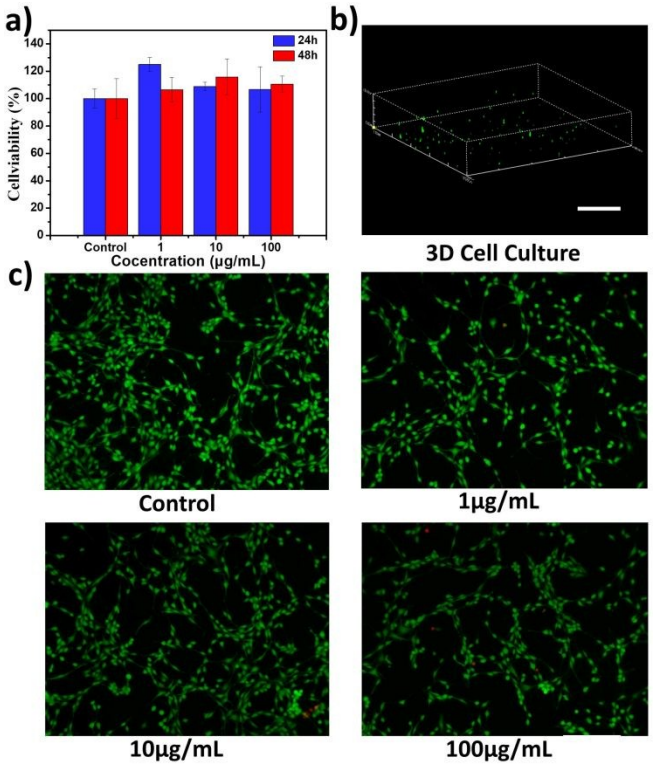

Fig. 5 (a) Cell viability of NIH-3T3 cells cultured with 0, 1, 10 and 100 μ g/mL^{-1} hydrogel powders, respectively. (b) Confocal images of 3D-cultured NIH-3T3 cells stained with AM-PI (scale bar = 400 μm). (c) Inverted fluorescence microscope images of NIH-3T3 cells stained with AM-PI after incubating with hydrogel powders (scale bar = 400 μm).

treatment with gel powders (Fig. 5c). And Fig. 5b showed that the cultured cells were distributed in a 3D form in the hydrogel. The results show that our hydrogels have the potential to be biological scaffolds.

In summary, we separate the printing process from the polymerization process by using a double-nozzle extrusion printing method. In this process, the enzymatic polymerization was initiated through the interdiffusion of enzyme and the substrate within xanthan gum frame, the hydrogel was enhanced owing to polymerization and the bioconjugate crosslinking. Moreover, our work provided a versatile method for hydrogel reinforcement——various natural polymer bio-inks containing amino or carboxyl groups could be cross-linked with the *N*-acryloyl-L-lysine without additional modification. The free radical polymerization mechanism and the amide cross-linking process were verified by EPR and IR. The final composite hydrogel showed adjustable mechanical strength. The double extrusion nozzle printed structure exhibited excellent fidelity, precision and clear structure. And the successful co-printing of lysine-based polymer hydrogels with viable cells confirms the low cytotoxicity of our system, which provides an all-biological printing method for soft tissue engineering and soft artificial organs.

This work was supported by the National Key R&D Program of China (No. 2018YFC1803100), the National Natural Science Foundation of China (No. 51873156) and the National Key R&D Program (No. 2016YFA0100800).

Conflicts of interest

View Article Online
DOI: 10.1039/D0CC00326C

There are no conflicts of interest to declare.

Notes and references

1 Q. Wang, Z. Yang, L. Wang, M. Ma and B. Xu, *Chem. Commun*., 2007, **10**, 1032-1034.
2 Q. Wang, Z. Yang, X. Zhang, X. Xiao, C. K. Chang and B. Xu, *Angew. Chem., Int. Ed*., 2007, **46**, 4285-4289.
3 Q. Wang, Z. Yang, Y. Gao, W. Ge, L. Wang and B. Xu, *Soft Matter*, 2008, **4**, 550-553.
4 Q. Wei, M. Xu, C. Liao, Q. Wu, M. Liu, Y. Zhang, C. Wu, L. Cheng and Q. Wang, *Chem. Sci.*, 2016, **7**, 2748-2752.
5 Q. G. Wang, Z. M. Yang, M. L. Ma, C. K. Chang and B. Xu, *Chem. - Eur. J.*, 2008,**14**,5073-5078.
6 H. Xie, J. Shao, Y. Ma, J. Wang, H. Huang, N. Yang, H. Wang, C. Ruan, Y. Luo, Q.-Q. Wang, P. K. Chu and X.-F. Yu, *Biomaterials*, 2018, **164**, 11-21.
7 A. Dawood, B. M. Marti, V. Sauret-Jackson and A. Darwood, *Br. Dent. J.*, 2015, **219**, 521-529.
8 K. Zhang, Z. Jia, B. Yang, Q. Feng, X. Xu, W. Yuan, X. Li, X. Chen, L. Duan, D. Wang and L. Bian, *Adv Sci*, 2018, **5**, 1800875.
9 Z. Zhao, S. Zhuo, R. Fang, L. Zhang, X. Zhou, Y. Xu, J. Zhang, Z. Dong, L. Jiang and M. Liu, *Adv. Mater.*, 2018, **30**, 1804435.
10 Z. Lin, M. Wu, H. He, Q. Liang, C. Hu, Z. Zeng, D. Cheng, G. Wang, D. Chen, H. Pan and C. Ruan, *Adv. Funct. Mater.*, 2019, **29**, 1808439.
11 X. Zhai, C. Ruan, Y. Ma, D. Cheng, M. Wu, W. Liu, X. Zhao, H. Pan and W. W. Lu, *Adv Sci*, 2018, **5**, 1700550
12 F. Xu, J. Celli, I. Rizvi, S. Moon, T. Hasan and U. Demirci, *Biotechnol. J.*, 2011, **6**, 204-212.
13 Y. Xu, D. Xia, J. Han, S. Yuan, H. Lin and C. Zhao, *Carbohydr. Polym.*, 2017, **177**, 210-216.
14 J. Leppiniemi, P. Lahtinen, A. Paajanen, R. Mahlberg, S. Metsa-Kortelainen, T. Pinornaa, H. Pajari, I. Vikholm-Lundin, P. Pursula and V. P. Hytonen, *ACS Appl. Mater. Interfaces.*, 2017, **9**, 21959-21970.
15 S. Rhee, J. L. Puetzer, B. N. Mason, C. A. Reinhart-King and L. J. Bonassar, *ACS Biomater. Sci. Eng.*, 2016, **2**, 1800-1805.
16 D. Chimene, K. K. Lennox, R. R. Kaunas and A. K. Gaharwar, *Ann. Biomed. Eng.*, 2016, **44**, 2090-2102.
17 I. Donderwinkel, J. C. M. van Hest and N. R. Cameron, *Polym. Chem.*, 2017, **8**, 4451-4471.
18 Y. Luo, A. Lode, M. Gelinsky, *Adv. Healthcare Mater*. 2013, **2**, 777-783.
19 R. K. Avery, H. Albadawi, M. Akbari, Y. S. Zhang, M. J. Duggan, D. V. Sahani, B. D. Olsen, A. Khademhosseini and R. Oklu, *Sci. Transl. Med.*, 2016, **8**, 365.
20 J. E. Kim, S. H. Kim and Y. Jung, *Tissue Eng Regen Med.*, 2016, **13**, 636-646.
21 S. Ahmad, M. Ahmad, K. Manzoor, R. Purwar and S. Ikram, *Int. J. Biol. Macromol.*, 2019, **136**, 870-890.
22 S. Shin, J. Y. Park, J. Y. Lee, H. Park, Y. D. Park, K. B. Lee, C. M. Whang and S. H. Lee, *Langmuir.*, 2007, **23**, 9104-9108.
23 M. Yamada, S. Sugaya, Y. Naganuma and M. Seki, *Soft Matter.*, 2012, **8**, 3122-3130.
24 R. Censi, S. van Putten, T. Vermonden, P. di Martino, C. F. van Nostrum, M. C. Harmsen, R. A. Bank and W. E. Hennink, *J. Biomed. Mater. Res., Part A.*, 2011, **97A**, 219-229.
25 W. Schuurman, P. A. Levett, M. W. Pot, P. R. van Weeren, W. J. A. Dhert, D. W. Hutmacher, F. P. W. Melchels, T. J. Klein and J. Malda, *Macromol. Biosci.*, 2013, **13**, 551-561.
26 C. M. Smith, J. J. Christian, W. L. Warren and S. K. Williams, *Tissue Eng.*, 2007, **13**, 373-383.
27 A. Skardal, J. Zhang, L. McCoard, S. Oottamasathien and G. D. Prestwich, *Adv. Mater.*, 2010, **22**, 4736-4740.
28 A. Skardal, J. Zhang, L. McCoard, X. Xu, S. Oottamasathien and G. D. Prestwich, *Tissue Eng Part A*, 2010, **16**, 2675-2685.
29 F. Gao, Z. Xu, Q. Liang, B. Liu, H. Li, Y. Wu, Y. Zhang, Z. Lin, M. Wu, C. Ruan and W. Liu, *Adv. Funct. Mater.,* 2018, **28**, 1706644.
30 S. Hong, D. Sycks, H. F. Chan, S. Lin, G. P. Lopez, F. Guilak, K. W. Leong and X. Zhao, *Adv. Mater.*, 2015, **27**, 4035-4040.
31 J. Wang, L. Lin, Q. Cheng and L. Jiang, *Angew. Chem., Int.Ed.*, 2012, **51**, 4676–4680.
32 D. Zhang, J. Yang, S. Bao, Q. Wu and Q. G. Wang, *Sci. Rep.*,2013, **3**, 1399-1405.
33 S. Faghihi, A. Karimi, M. Jamadi, R. Imani and R. Salarian, *Mater. Sci. Eng., C*, 2014, **38**, 299-305.
34 L.S. Jang and H.-K. Keng, *Biomed Microdevices.*, 2008, **10**, 203-211.

35 T. Su, Z. Tang, H. He, W. Li, X. Wang, C. Liao, Y. Sun and Q. Wang, *Chem. Sci.*, 2014, **5**, 4204-4209.

View Article Online
DOI: 10.1039/D0CC00326C